Color Modification of Spinel by Nickel Diffusion: A New Treatment

Michael Jollands, Abadie Ludlam, Aaron C. Palke, Wim Vertriest, Shiyun Jin, Pamela Cevallos, Sarah Arden, Elina Myagkaya, Ulrika D'Haenens-Johannson, Vararut Weeramongkhonlert, and Ziyin Sun

A set of faceted spinel with blue to green hues, marked as "cobalt diffused," were obtained by researchers from GIA in Bangkok. Analyses of the absorption, luminescence, and chemistry of the stones have revealed that they were not diffused with cobalt, but instead with nickel. Laser ablation–inductively coupled plasma–mass spectrometry indicated high nickel concentrations (tens of thousands of ppma) at the edge of the stones, and a compositional traverse across one spinel showed a decrease of nickel toward the core, consistent with diffusion treatment. The trace element concentrations in the cores were consistent with natural spinel, as were the refractive indices. A similar decrease in lithium concentration was also seen, suggesting that treatment was done in the presence of a flux melt. Absorption spectra recorded in the ultraviolet/visible/near-infrared region contained characteristic bands at 369, 381, 475, 597, and 639 nm. Annealing experiments conducted on one spinel demonstrated that the 475 nm band is sensitive to the oxygen partial pressure (pO_2) in the experiment. The band increases in intensity following a high-pO_2 anneal, then decreases following an anneal at low pO_2. Photoluminescence spectra were consistent with heated natural spinel. This treatment now exists in the gem market and should be considered a possibility in spinel with blue or green hues.

In November 2022, a parcel of 24 spinels weighing approximately 0.51–1.19 ct and described as "cobalt diffused" was obtained by the research team at GIA in Bangkok. Of these, eight possessed the deep blue color characteristic of cobalt diffusion, while the others had lighter blue, greenish blue, bluish green, or blue-green color (figure 1). Wafers were cut from the core of several stones, and all showed diffuse color zonation, from more blue/green at the rim to near-colorless at the core (figure 2).

The concentrations of various elements were recorded along culet-to-table transects in the wafers using laser ablation–inductively coupled plasma–mass spectrometry (LA-ICP-MS). The expectation was that all stones would show simple cobalt diffusion profiles, meaning high cobalt concentrations at the edge, changing gradually to lower concentrations in the core. This has been well described by Saeseaw et al. (2015), Peretti et al. (2015), and Krzemnicki et al. (2017). For the deep blue stones, the result was as expected: high cobalt, thousands of atomic parts per million (ppma) at the rim, changing gradually to low cobalt in the core. This is clear evidence of cobalt diffusion treatment. However, all other stones (i.e., those that were not deep blue) showed something quite different. The cobalt concentration in these crystals was negligible, generally below a few atomic ppm. The nickel concentration, conversely, was extremely elevated, generally around 10000 to 20000 ppma at the rim and dropping to a few ppma in the core. An initial conclusion was that these "cobalt-diffused" spinels were actually nickel diffused. Sub-

In Brief

- Nickel-diffused spinel was discovered in a parcel of spinel marked as "cobalt diffused."
- The diffusion treatment was likely conducted in the presence of a nickel-bearing flux melt, in an oxidizing atmosphere such as air or oxygen gas, potentially at temperatures exceeding 1500°C.
- This treatment can be readily identified by high nickel content and the presence of bands at 597 and 639 nm in absorption spectroscopy.

See end of article for About the Authors.
Gems & Gemology, Vol. 59, No. 2, pp. 164–181,
http://dx.doi.org/10.5741/GEMS.59.2.164

Figure 1. Suite of faceted nickel-diffused spinel (0.67–1.01 ct) showing a range of color from blue to bluish green. Photo by Aaron Palke and Diego Sanchez.

sequent investigations using various absorption, luminescence, and fluorescence techniques along with gemological observations confirmed that the samples were indeed nickel diffused and that natural near-colorless spinel was likely used as the starting material. Additionally, nickel was confirmed to be the main chromophore responsible for the modified color. These observations are described in detail below, along with the results of some preliminary experiments on the diffused stones, discussion of heat treatment methods, and some potential identification criteria.

Figure 2. Wafers cut from the center of a nickel-diffused spinel (top) and a cobalt-diffused spinel (bottom). The cobalt-diffused stone was in the same parcel as the nickel-diffused stones, showing a clearly different hue and color intensity. Photos were taken using a Nikon SMZ1500 microscope with the wafers placed on a white diffuser plate.

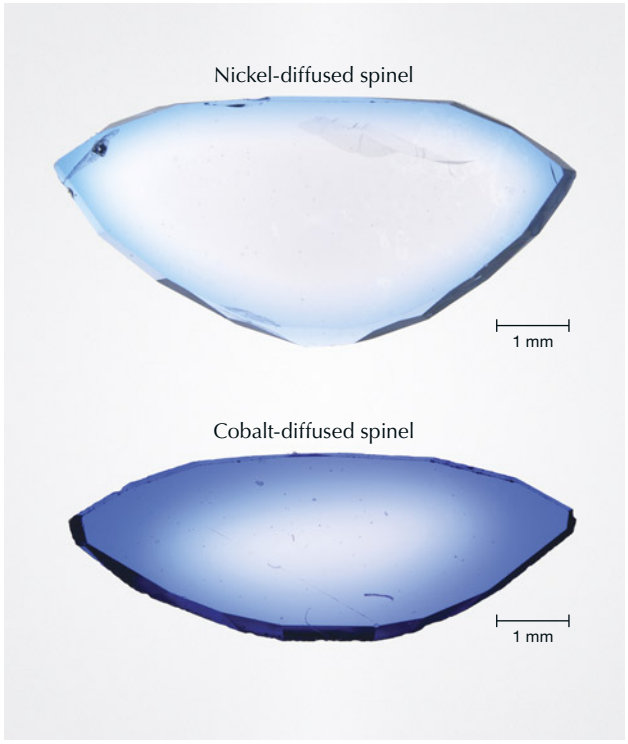

MATERIALS AND METHODS

Materials. Twenty-four faceted spinel samples were purchased by GIA Bangkok for scientific examination. These were all oval cut and weighed between 0.51 and 1.19 ct. Eighteen of them (thirteen nickel-diffused and five cobalt-diffused) were left in their original faceted state, but three nickel-diffused and three cobalt-diffused stones were fabricated into doubly polished wafers perpendicular to the table. The wafers were polished on both faces using a tin alloy lap impregnated with 6 µm diamond paste. Colors, weights, and forms (faceted or wafer) of the nickel-diffused stones are presented in table 1.

Analytical Methods. *Gemological Testing*. A total of 16 stones were studied using standard gemological methods at GIA in New York, Carlsbad, and Bangkok. The eight stones in the original parcel that were clearly cobalt diffused were not studied beyond identification of cobalt diffusion treatment. Refractive indices were measured on faceted stones and on doubly polished wafers using a GIA-built refractometer. The fluorescence reactions to both long-wave (365 nm) and short-wave (254 nm) UV light were de-

TABLE 1. The 16 nickel-diffused spinel samples analyzed for this study.

Sample no.	Color[a]	Original (faceted) weight (ct)	Form
17407059	Greenish blue	0.861	Faceted oval
17407060	Greenish blue	0.764	Faceted oval
17407068	Blue	0.674	Faceted oval
17407066	Greenish blue	0.940	Faceted oval
17407062	Greenish blue	0.895	Faceted oval
17407061	Blue	0.906	Faceted oval
17407070	Blue	1.009	Faceted oval
17407067	Bluish green	0.812	Faceted oval
17407058	Bluish green	1.045	Faceted oval
17407064	Green	0.884	Faceted oval
17407065	Green	0.940	Faceted oval
17407071	Greenish blue	0.850	Faceted oval
17407072	Greenish blue	0.553	Faceted oval
17407057[b]	Greenish blue	0.513	Wafer
17407126	Greenish blue	0.513	Wafer
17407123	Bluish green	1.192	Wafer
17407124[c]	Blue	0.827	Wafer
17407069	Blue	0.827	Wafer

[a]*Color was assessed visually on faceted stones.*
[b]*17407057 and 17407126 were both cut from one stone.*
[c]*17407124 and 17407069 were both cut from one stone.*

termined using mercury lamps. Additionally, faceted stones were viewed through a Chelsea color filter and also immersed in methylene iodide in order to observe internal color variations.

Energy-Dispersive X-ray Fluorescence (EDXRF). EDXRF spectra were recorded at GIA in Carlsbad by placing faceted stones in a Thermo Quant'X EDXRF spectrometer, operating at 12 kV and 1.92 mA, with an aluminum filter. Fluorescence was recorded between 0 and 40 keV. These data are not quantified, so no detection limits are provided.

LA-ICP-MS. LA-ICP-MS data were recorded using a Thermo iCAP Q ICP-MS coupled to an Elemental Scientific 213 nm (Nd:YAG) laser ablation system via helium carrier gas. This was done using three identical LA-ICP-MS systems, at GIA in New York, Carlsbad, and Bangkok. Most stones were analyzed by ablating 35 µm circular spots on the girdles, at 20 Hz, with a ~11 J/cm^2 fluence. The doubly polished wafers were ablated using the same conditions, but on one of the two main polished faces rather than on the girdle, and using a 50 µm circular spot with a centroid located at approximately 50 µm from the edge on the table side.

The analyzed elements (isotopes in parentheses) were lithium (^{7}Li), beryllium (^{9}Be), magnesium (^{25}Mg), aluminum (^{27}Al), titanium (^{47}Ti), vanadium (^{51}V), chromium (^{53}Cr), manganese (^{55}Mn), iron (^{57}Fe), cobalt (^{59}Co), nickel (^{60}Ni and/or ^{62}Ni), zinc (^{66}Zn), and gallium (^{69}Ga). Dwell times were between 0.01 and 0.05 s per isotope. To record a compositional transect across one doubly polished stone, the sample was moved below a stationary, continuously ablating 40 µm circular spot, with 20 Hz repetition rate and fluence around 7 J/cm^2, while the ICP-MS counted continuously. Dwell times for the transect were 0.05–0.10 s per isotope, analyzing the same isotopes as listed above. Magnesium was not quantified in any analysis, but the compositional transect shows resolvable magnesium variation when calculated as magnesium/aluminum (counts per second), which can still be used to understand relative magnesium concentrations along the transect.

In all cases, background analyses were recorded for around 1 minute. The primary standard was NIST SRM 610 glass, using the reference values from Jochum et al. (2011). Data were processed using Iolite software (Paton et al., 2011), with ^{27}Al as the internal standard, initially assuming a constant value of 39.7 wt.%. This implicitly assumes that nickel incorporation into spinel is accomplished by removal of magnesium rather than aluminum.

Detection limits were determined for each analysis using the Longerich et al. (1996) method, generally using at least 30 s of manually selected background. Minimum and maximum detection limits for all analyses, for each element, were: lithium: 0.1–0.6 ppma; beryllium: 0.1–0.5 ppma; titanium: 0.04–0.2 ppma; vanadium: 3–84 ppba; chromium: 0.06–0.36 ppma; manganese: 9–140 ppba; iron: 0.4–1.9 ppma; cobalt: 2–30 ppba; nickel: 0.05–0.4 ppma; zinc: 13–68 ppba; and gallium: 2–12 ppba. No correction was made for the decreasing aluminum content by weight associated with an increased nickel content. This is necessary for accurately determining concentrations by weight, given the difference in atomic mass between nickel and magnesium (58.69 u and 26.98 u, respectively), again assuming that nickel incorporation is associated with magnesium removal. The justification is that even at around 5 wt.% nickel, the highest measured in this study, the discrepancy between actual concentrations and calculated concentrations is <3% (figure 3). Additionally, making this correction would require *a priori* assumptions about valence state and coordination environment of nickel, which cannot be confidently made.

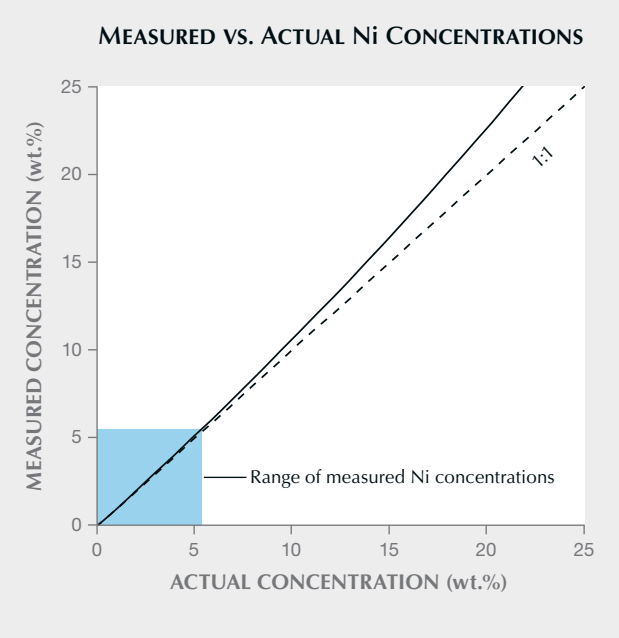

Figure 3. Calculated discrepancies arising from the assumption that spinel is pure $MgAl_2O_4$, then using the appropriate value for the aluminum concentration (39.7 wt.%) as an internal standard when reducing LA-ICP-MS data recorded from stones with high nickel (in wt.%). The x-axis shows the actual nickel concentration, and the y-axis shows the concentration that would be calculated using this internal standard value. At high concentrations, the nickel becomes systematically overestimated. The same degree of overestimation would be seen for all analyzed elements. In these stones, the nickel concentrations are still low enough (blue box) that the maximum inaccuracy from this calculation is around 3% in the most extreme case.

In addition to collecting LA-ICP-MS data from the nickel-diffused stones in this study, we extracted data from a larger GIA database, from analyses of blue, green, green-blue, bluish green, and greenish blue spinel determined to be natural. This yielded 1,495 individual analyses. These data were compiled for comparison with data from the diffused stones.

Energy-Dispersive Spectroscopy (EDS) Mapping. EDS spectra were recorded from sample 17407069 following gold-coating, using an Oxford X-Max^N 20 EDS detector on a Zeiss EVO Ma 10 scanning electron microscope at GIA in New York, operating at 15 keV accelerating voltage, 30 nA current, and 71× magnification. The pixel dwell time was 60 µs. Counts

were extracted from spectra as the maxima on the Kα bands of oxygen, aluminum, magnesium, and nickel. Post-processing was done on the extracted X-Y-counts matrices using MATLAB. Due to the large size of the area being mapped and analytical limitations, the total count rate was not constant; therefore, all counts on aluminum, magnesium, and nickel were normalized to counts on oxygen. Additionally, a swath of data (400 × 1291 point rectangle) was extracted from the larger data matrix along a table-to-culet transect and averaged parallel to the table, to give one-dimensional transects of oxygen-normalized counts.

Ultraviolet/Visible/Near-Infrared (UV-Vis-NIR) Spectroscopy. UV-Vis-NIR spectra were recorded in absorbance mode between 200 and 1500 nm from five doubly polished wafers using a Perkin Elmer Lambda 950 UV-Vis spectrometer at GIA in New York. Four of the wafers were nickel diffused (samples 17407057, 17407124, 17407123, and 17407126), and one was cobalt diffused (17407125), with the latter analyzed for comparison only. The wafers were mounted onto an aluminum plate containing a 0.5 mm circular aperture located as close as possible to the stone's edge. For the sample that was annealed experimentally (17407067), spectra were recorded from the whole stone using a using a custom-built UV-Vis system at GIA in Carlsbad, operating in transmission mode from 250 to 980 nm, with an integrating time of 3000 ms and 3 accumulations.

Photoluminescence (PL) Spectroscopy. PL spectra were recorded from 630 to 750 nm on the core and rim of one doubly polished wafer (sample 17407124) using a Renishaw inVia Raman microscope with a 514 nm laser, 1800 l/mm grating, and a 5× objective at GIA in New York. The power and counting times were adjusted to obtain maximum signal while avoiding saturation. The high concentration of nickel appeared to be associated with quenched fluorescence, which meant that higher power and longer accumulation times were required for spectra recorded near the high-nickel rim.

Diffusion Modeling. Diffusion is described using Fick's first and second laws, two partial differential equations that can be thought of as defining the way in which particles spread out over space and time. In order to apply these laws to a real situation, the equations must be solved for a given set of conditions, which require approximations to be made regarding the geometry of the system (e.g., a stone) and the nature of the source of diffusing species (e.g., a high-nickel powder or melt placed into contact with the stone). The aim here is to determine Dt, which is the diffusion coefficient (D, in units of square meters per second, m^2/s) multiplied by the time (t, in units of seconds, s). In this case, the diffusion coefficient is a number that describes how rapidly a given element, such as nickel, moves through spinel.

In order to determine diffusion coefficients from the LA-ICP-MS transect, concentration vs. distance data were fitted to the solution of Fick's second law describing diffusion in a one-dimensional semi-infinite medium, using a constant boundary condition (Crank, 1975):

$$C(x,t) = C_{core} + (C_{rim} - C_{core})\,erfc\frac{x}{2\sqrt{Dt}} \quad (1)$$

In this equation, x is the distance (in meters, m) from the edge, C is the concentration (in ppma) at the core (C_{core}) and rim (C_{rim}) at a given distance at a given time ($C(x,t)$), and $erfc$ is the complementary error function.

This fitting was only done for half profiles, meaning the data were recorded from the core to the table, instead of table-to-culet or core-to-culet. This is because the shape of the culet renders this solution to Fick's second law inappropriate—the solution is strictly valid only for a plane sheet with infinite extent. The flat table of a faceted stone is a reasonable approximation of this geometry, but the culet is not. The data was fitted to the model using nonlinear least squares regression implemented in MATLAB, with the output being Dt (units of m^2). These Dt values are presented as their base-10 logarithm.

Experimental Methods. To complement analyses on the as-received stones, one faceted spinel (sample 17407067, bluish green) was annealed at various temperature (T) and oxygen partial pressure (pO_2) conditions, and then UV-Vis spectra were recorded on the whole spinel after each step. The aim was to determine whether temperature and oxygen partial pressure could modify the defects present in the stone, and therefore potentially the color. Pure O_2 at atmospheric pressure has pO_2 = 1 atm. The O_2 content in air is 21%, and therefore pO_2 = 0.21 atm. The pO_2 can also be controlled by mixing gases. In one experiment, the furnace was filled with a mixture of CO_2 and H_2

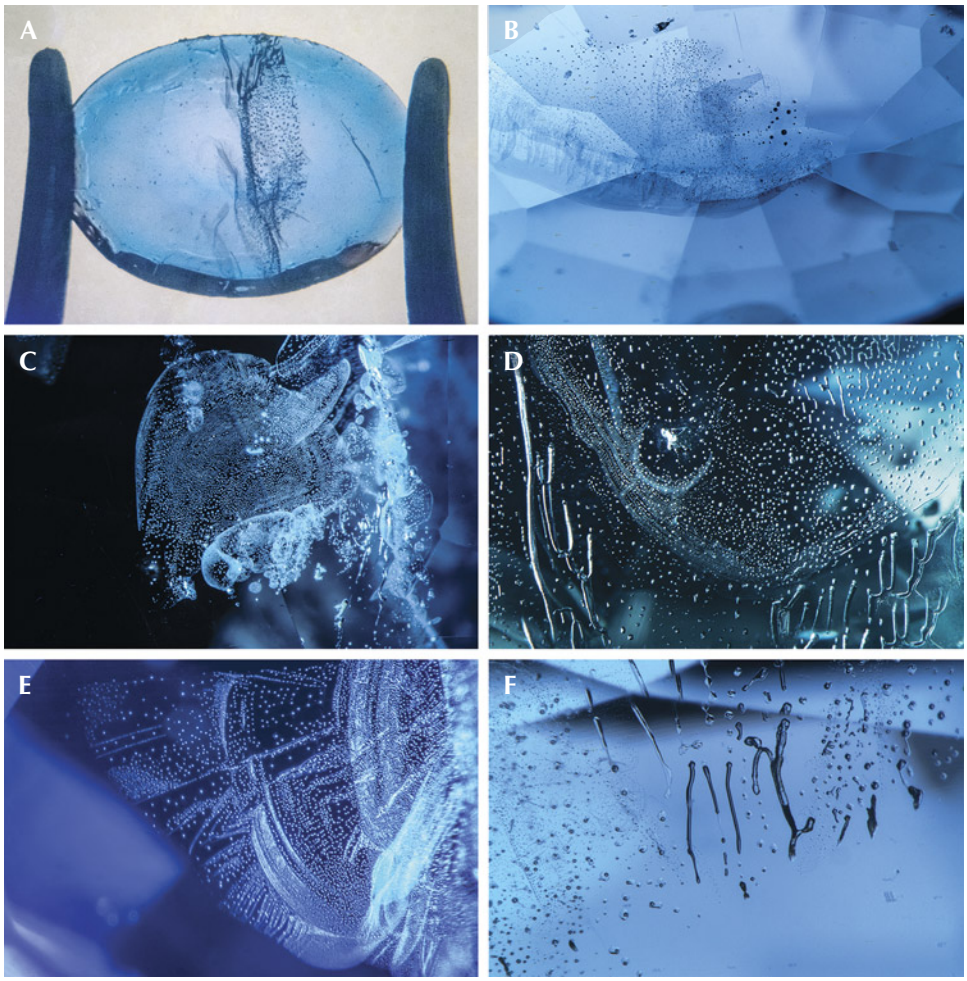

Figure 4. Nickel-diffused spinel shows subtle color concentration along facet junctions (A and B) and features suggesting flux-assisted healing of the fractures during the heating process (C–F). Photos by Aaron Palke; fields of view 10.24 mm (A), 2.90 mm (B), 2.34 mm (C and D), 1.76 mm (E), and 1.99 mm (F).

gases, which react to form CO, H_2O, CH_4, and O_2, yielding a very low partial pressure of O_2. A 2:1 mix of CO_2:H_2 was used, giving $pO_2 = 4 \times 10^{-6}$ atm at 1750°C (Prunier and Hewitt, 1981). Experiments were conducted in a 1000-3560-FP24 Thermal Technology gas mixing furnace. The temperature/time/pO_2 annealing conditions, for sequentially heating the same stone, were: (1) 1100°C for 10 hours at 1 atm, (2) 1700°C for 18 hours at 1 atm, and (3) 1750°C for 40 hours at 4×10^{-6} atm.

RESULTS

Gemological Observations. Gemological observations were consistent with spinel. Refractive indices for the nickel-diffused samples were generally 1.718, but some samples had values as high as 1.725, possibly due to the increased concentration of nickel at the surface. All samples were inert to long-wave UV light. Most were also inert to short-wave UV, but a few showed faint chalky yellow fluorescence near the edges when prepared as doubly polished wafers. All faceted stones had a weak to strong red reaction when viewed through the Chelsea color filter. The doubly polished wafers viewed in this way showed color zonation: red at the rim and colorless in the center.

When immersed in methylene iodide, the faceted stones displayed a strong concentration of color around the rim of the stone (figure 4A), sometimes with additional subtle color concentration along the facet junctions (figure 4B). Microscopic observations sometimes revealed this same color concentration along facet junctions, particularly at the keel of the stones, although the effect was more subtle here than in other treated material, such as titanium-diffused sapphire. The most striking microscopic feature was the abundance of artificially healed fractures, likely associated with the presence of a flux material during heating (figure 4, C–F). This is also supported by the trace element data, described below, which show

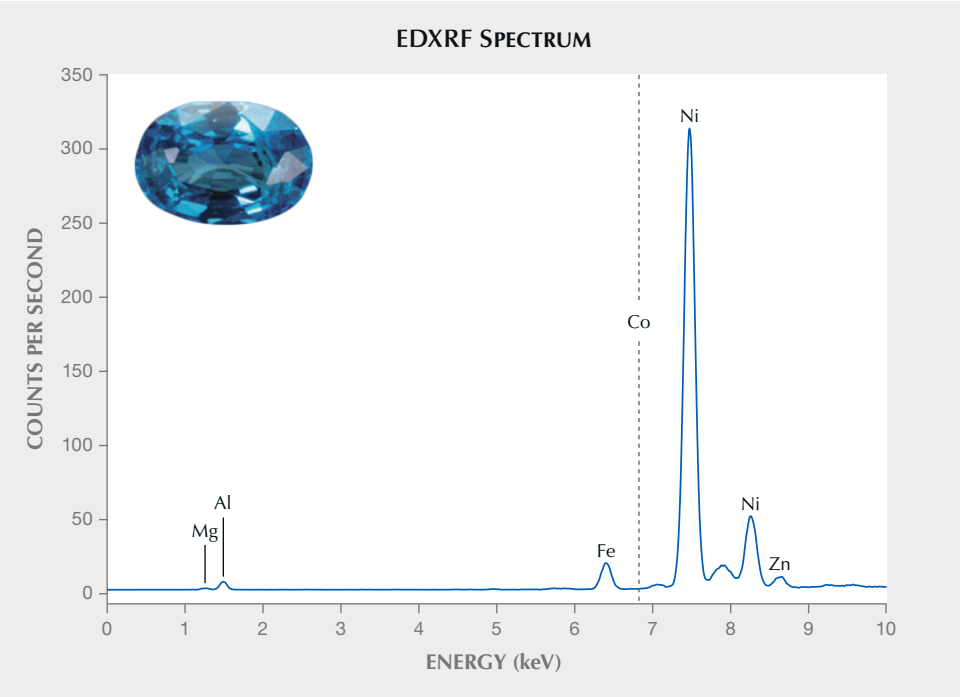

Figure 5. An EDXRF spectrum of a nickel-diffused spinel (sample 17407067) acquired at 12 kV with an aluminum filter. Distinct nickel fluorescence peaks are visible. The position of the main cobalt peak, absent in this spectrum, is shown by the dashed line.

high amounts of lithium at the stones' edge—lithium is a common component of flux material.

Compositional Analysis. *X-ray Fluorescence.* EDXRF spectra of nickel-diffused stones (e.g., figure 5) consistently showed the strongest bands at 7.47 keV, interpreted as the sum of the nickel Kα lines ($K\alpha_1$ and $K\alpha_2$ at 7.48 and 7.46 keV, respectively), with an associated Kβ band at 8.26 keV. No nickel L lines are visible in figure 5. Also clearly visible are Mg Kα (1.25), Al Kα (1.48), Fe Kα (6.40), Fe Kβ (7.06), and Zn Kα (8.64). No Co Kα line is visible at 6.93 keV.

LA-ICP-MS. *Single Point Analyses*. Table 2 shows the concentrations of measured trace elements, measured either on the girdle of as-received faceted stones or at around 50 µm from the table in doubly polished wafers. The concentration of nickel at the edge of the spinel was high, around 10000–20000 ppma. These nickel concentrations are very high compared to natural gem-quality spinel submitted for analyses at GIA (figure 6A). It should be noted, however, that the nickel end member of the spinel group (chihmingite, $NiAl_2O_4$) does exist in nature (Miyawaki et al., 2022).

Along with elevated nickel, some but not all stones also contained high lithium concentrations, up to around 3000 ppma at the surface (see table 1). Such high lithium is rare in natural, untreated gem spinel (figure 6B). Concentrations of other elements, even if added or removed during the diffusion treatment, were generally within normal ranges for gem spinel. Notably, this also includes beryllium (figure 6C), despite the increasing concentration of beryllium toward the edge in the LA-ICP-MS transect, described below (figure 7).

Additionally, the concentrations of all other measured elements (titanium, vanadium, chromium, manganese, iron, cobalt, zinc, and gallium) were highly variable between stones. Preliminary analyses from the cores of other doubly polished wafers (samples 17407047, 17407126, 17407123, and 17407069) showed different concentrations of elements other than nickel (see table 2) in areas apparently unaffected by diffusion, suggesting that these concentration variations relate at

Figure 7 (opposite page). Concentrations of magnesium, nickel, lithium, iron, zinc, vanadium, titanium, beryllium, manganese, gallium, chromium, and cobalt recorded along a ~3.3 mm culet-to-table transect across a wafer cut from the core of a nickel-diffused spinel (sample 17407124). Magnesium is not quantified, so the y-axis in the top right plot is arbitrary. Notably, nickel shows an extreme concentration decrease from rim to core, whereas cobalt shows a very small decrease with sub-ppm concentration along the whole transect. The transects for elements showing clear concentration changes are replotted in figure 12 for the purpose of diffusion modeling.

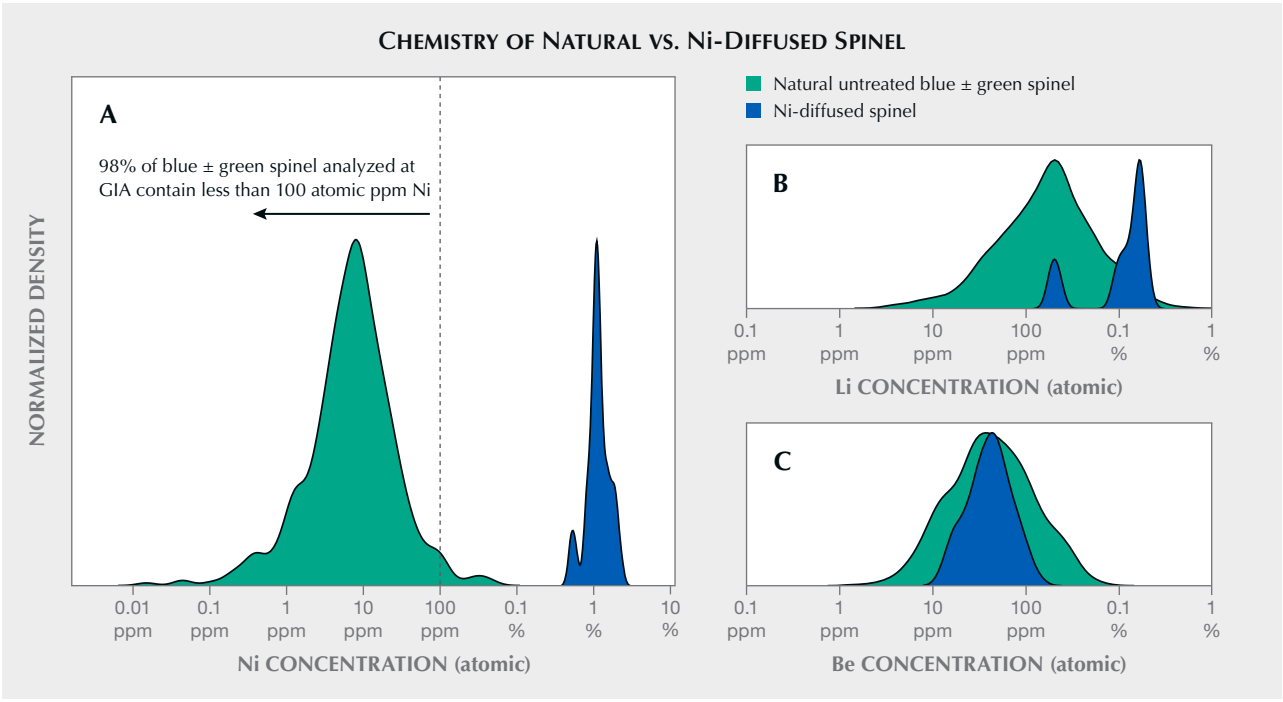

Figure 6. A: Kernel density plots of nickel concentrations measured on the girdles of nickel-diffused stones, along with the range of nickel concentrations seen in a subset of spinel (1,495 analyses) submitted to GIA. This subset includes natural, untreated spinel with the following hues: blue, greenish blue, green-blue, blue-green, and bluish green. The nickel concentrations are considerably higher (100–10,000×) in the nickel-diffused stones. Also shown are the concentrations of lithium (B) and beryllium (C), both of which are also elevated at the rims, as shown in the LA-ICP-MS transect (figure 7). Lithium concentrations in diffused stones are generally higher than the natural range, but beryllium concentrations are indistinguishable between natural untreated spinel and nickel-diffused spinel.

least partially to different starting materials (i.e., different natural spinel) rather than different treatment conditions. At this point, however, we cannot confidently describe the nature of the starting materials.

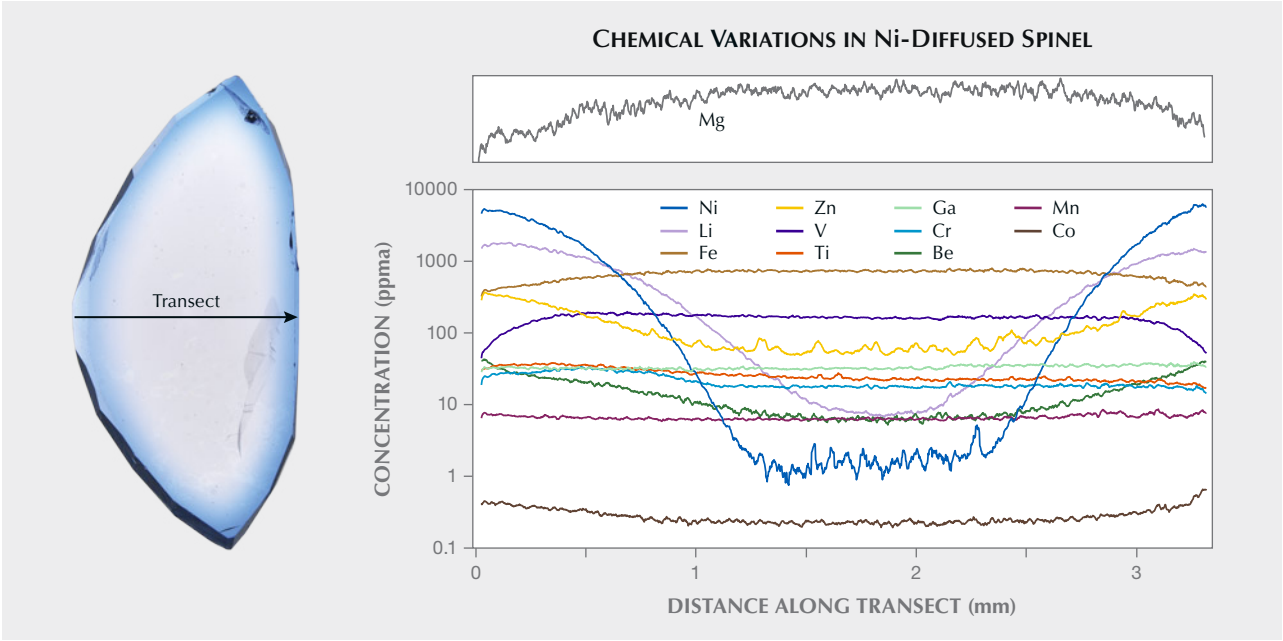

TABLE 2. Concentrations of trace and minor elements in nickel-diffused spinel (in ppma), measured using LA-ICP-MS on the girdle or near the edge of the spinel.[a]

Sample no.	Li	Be	Ti	V	Cr	Mn	Fe	Co	Ni	Zn	Ga
17407059	924	79.0	5.9	19.1	5.9	16.9	183	1.4	13929	250	50
17407060	1084	44.7	13.3	16.7	17.8	14.6	174	1.1	17840	360	40
17407068	1980	90.4	9.7	22.9	147.4	24.1	396	12.9	18995	925	66
17407066	1208	28.2	13.8	29.1	3.8	6.7	182	0.6	8194	276	33
17407062	185	31.0	3.2	19.0	0.9	14.2	180	1.2	19030	474	45
17407061	1617	58.8	19.6	7.1	36.5	27.0	473	1.3	10746	150	36
17407070	192	32.5	7.7	13.3	15.3	13.1	349	0.8	12021	288	43
17407067	1343	69.9	8.0	29.6	5.3	38.5	420	1.1	14857	286	50
17407058	222	16.6	5.0	13.8	18.5	6.0	169	0.7	10339	410	42
17407064	1631	51.0	9.0	7.0	10.4	12.1	433	0.9	11399	458	56
17407065	1773	26.5	6.6	7.4	12.0	8.9	333	0.6	10123	512	64
17407071	1649	49.0	9.4	5.0	45.1	33.6	578	0.8	9961	204	34
17407072	1640	41.5	29.4	6.9	54.3	28.8	500	0.8	11601	249	41
17407057	899	16.3	7.7	98.8	30.6	6.4	6	0.5	5794	451	64
17407126	1024	18.2	8.5	98.3	29.4	5.9	7	0.5	5177	478	59
17407023	1338	116.9	15.7	7.8	15.8	62.1	13	0.4	4977	292	79
17407024	1722	36.8	18.2	69.8	19.2	10.9	14	0.8	7854	334	45
17407069	1573	40.2	18.7	53.6	15.1	10.2	16	1.3	8298	330	42

[a]*Concentration values are means of 2–3 analyses. Concentrations in the last five samples were measured on doubly polished wafers using 50 µm diameter circular LA-ICP-MS spots with centroids 50 µm from the edge of the spinel closest to the table. All others were measured using a 35 µm spot on the girdle on faceted stones.*

These data show that nickel appears to be a weak chromophore, as thousands to tens of thousands of ppma led to relatively weak colors. In contrast, cobalt diffusion treatment requires only a few hundred to thousands of ppma cobalt to create deep blue colors (e.g., Saeseaw et al., 2015; Krzemnicki et al., 2017). This may relate to the incorporation mechanism of nickel, described below (in the "Nickel Incorporation Mechanism and Valence State" section).

Concentrations Recorded Along a Transect. In one stone where trace element concentrations were recorded along a central transect (sample 17407124), nickel, lithium, beryllium, zinc, manganese, and cobalt show decreasing concentrations from the rim to the core (figure 7), with U-shaped profiles. The largest concentration change is associated with nickel, from ~1 ppma in the core to ~5000 ppma at the rim. Cobalt shows the smallest change, from ~0.4 ppma at the core to ~0.8 ppma at the rim. Conversely, vana-

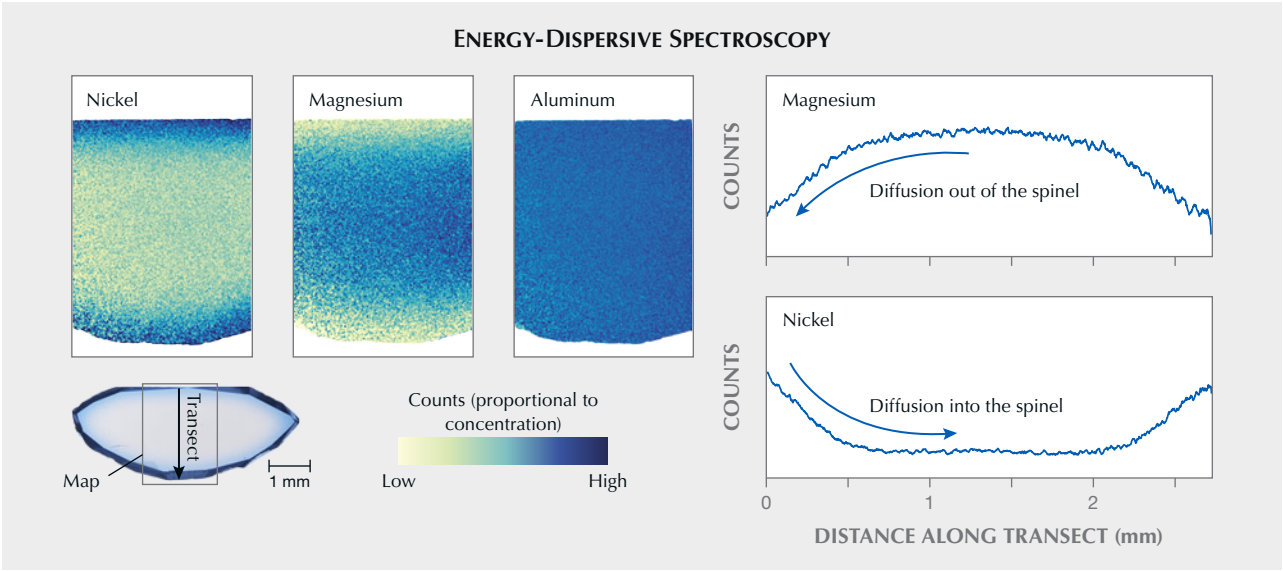

Figure 8. Maps of nickel, magnesium, and aluminum recorded by EDS from sample 17407069. Colors represent counts on nickel, magnesium, and aluminum normalized to total signal intensity by dividing by counts on oxygen (all Kα lines). The normalization was necessary given nonconstant total signal across the mapped area. Color scales are set to maximize contrast; the ranges (normalized to oxygen) are 0–0.04 for nickel, 0.85–1.2 for magnesium, and 1–2.6 for aluminum. Also shown are profiles of magnesium and nickel, extracted from the maps in table-culet transects.

dium, iron, and magnesium display inverted U-shaped profiles—i.e., lower concentrations at the rim than at the core. The magnesium profile is displayed separately, as this cannot be accurately quantified when using NIST SRM 610 as a primary standard and aluminum as the internal standard. The likely reason is that the magnesium concentration in the NIST SRM 610 standard glass is around three orders of magnitude lower than in the spinel. As a result, using the analytical and data reduction routine described above, the quantified magnesium content is about 30% lower than expected. This is not problematic for estimating diffusion coefficients, though. Chromium and titanium show variable concentrations, but neither has a clear U-shaped or inverted U-shaped profile. Gallium shows no apparent concentration change.

EDS. EDS has considerably higher spatial resolution than LA-ICP-MS but suffers from much poorer detection limits, so the only elements that could be measured were nickel, magnesium, aluminum, and oxygen (figure 8). Nickel shows a clear concentration decrease from rim to core. Magnesium shows the opposite, which is discussed later, and aluminum shows no apparent zonation. The zonation pattern of nickel conforms to the faceted stone's shape.

UV-Vis-NIR Spectroscopy. UV-Vis-NIR spectra recorded from the rims of double-polished wafers recovered from as-received stones show main peaks at 369, 381, 475, 597, and 639 nm (figure 9). These positions are consistent with those present in spectra recorded from nickel aluminate powders synthesized for use as cyan dyes (Serment et al., 2020), nickel-doped single-crystal spinel (Jouini et al., 2007), and nickel-doped gahnite ($ZnAl_2O_4$; Lorenzi et al., 2006). Figure 9 also shows a spectrum recorded from a cobalt-diffused spinel, obtained in the same parcel as these nickel-diffused crystals, showing clearly different absorption band positions.

Following the experimental anneal at 1100°C in pure O_2 (10 hours), the 475 nm band increased in intensity relative to the as-received stone (figure 10). There was no clear change in the intensity of the 369, 381, 597, and 639 nm bands. There was no apparent change in the spectra following a subsequent higher-temperature anneal in pure O_2 at 1700°C (18 hours). Following the 1750°C anneal in a low-pO_2 2:1 CO_2-H_2 mix (40 hours), however, the 475 nm band was completely eliminated and the intensity of the 369, 381, 597, and 639 nm bands decreased considerably, as did the overall absorbance. This is consistent with the final color, which was a much lighter blue than the original stone.

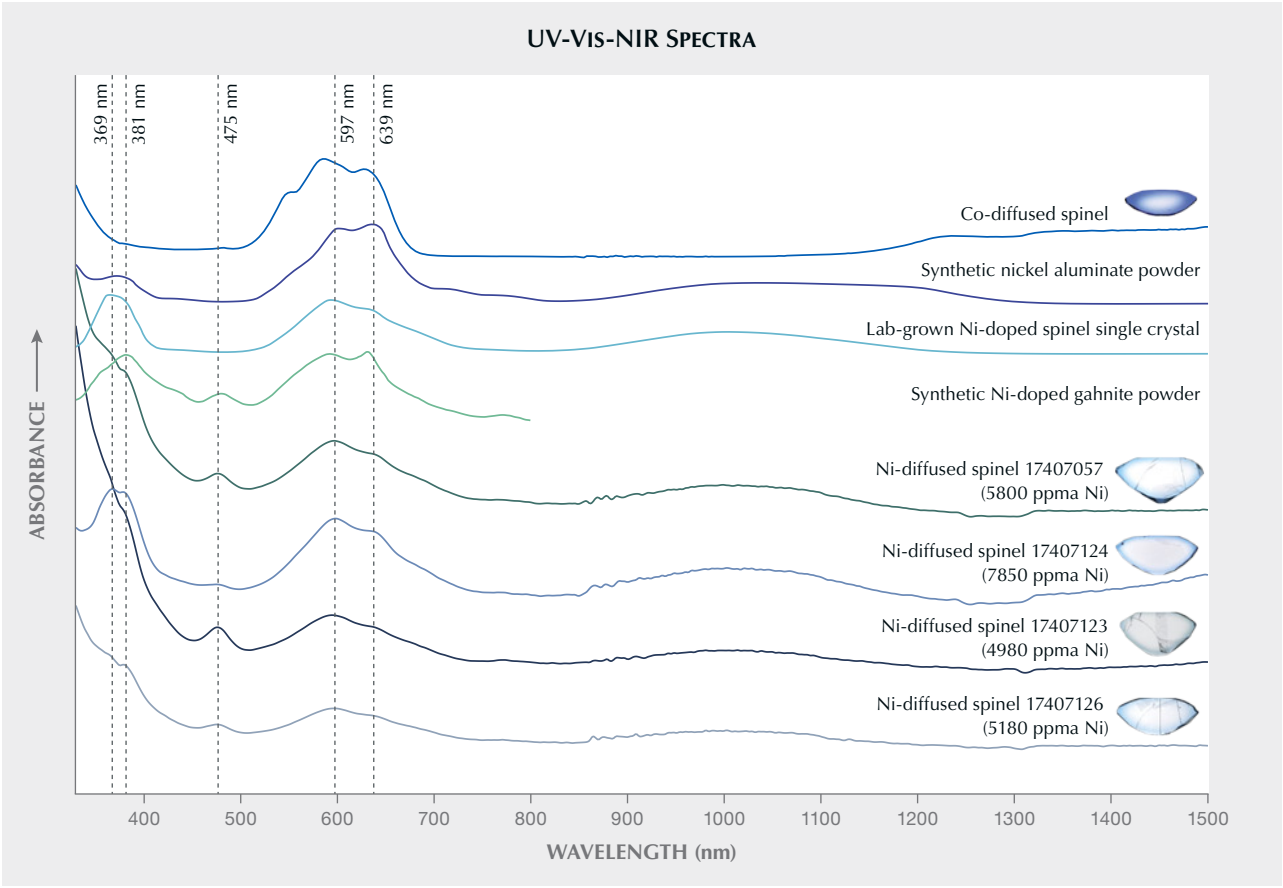

Figure 9. UV-Vis-NIR spectra recorded from the near-rim regions of doubly polished wafers fabricated from nickel-diffused spinel (bottom four curves). These were recorded by placing the stone over a 0.5 mm circular aperture, located as close as possible to the stone's edge at the table. Images of the stones are shown. Also presented are concentrations of nickel recorded using a 50 µm LA-ICP-MS spot, centered at 50 µm from the stone's edge at the table. This gives an approximation of the relative nickel concentration between stones, but is likely an overestimation of the mean nickel concentration in the area from which the UV-Vis-NIR spectrum was recorded given the nature of the nickel concentration gradients. Also shown are spectra recorded from a synthetic nickel aluminate ($NiAl_2O_4$; Serment et al., 2020), a single crystal of nickel-doped spinel (Jouini et al., 2007), a synthetic nickel-doped gahnite ($ZnAl_2O_4$) powder (Lorenzi et al., 2006), and a cobalt-diffused spinel. The positions of the main bands in the nickel-diffused material are denoted by dashed lines. Spectra are offset for clarity.

PL Spectroscopy. PL spectra recorded with 514 nm excitation are shown in figure 11. Spectra of the nickel-diffused stones are similar to those of heat-treated natural spinel (Widmer et al., 2015), which is in line with visual observations of inclusions and refractive indices. As with most natural spinel, the spectra are dominated by bands attributed to chromium. The spectra show broadening of the band(s) at around 686 nm.

PL spectra recorded near the spinel rims are different from those recorded in the cores, with the rim spectra showing a dominant band at 687.5 nm and core spectra showing a strong doublet with maxima at 685.6 and 687.3 nm. This difference in PL spectra may be associated with nickel, but it is notable that a spectrum recorded from a natural, unheated spinel with relatively high nickel (around 350 ppma) from GIA's production database did not clearly display this feature. Spectra recorded from faceted stones using nonconfocal PL spectroscopy will likely show some combination of these spectra.

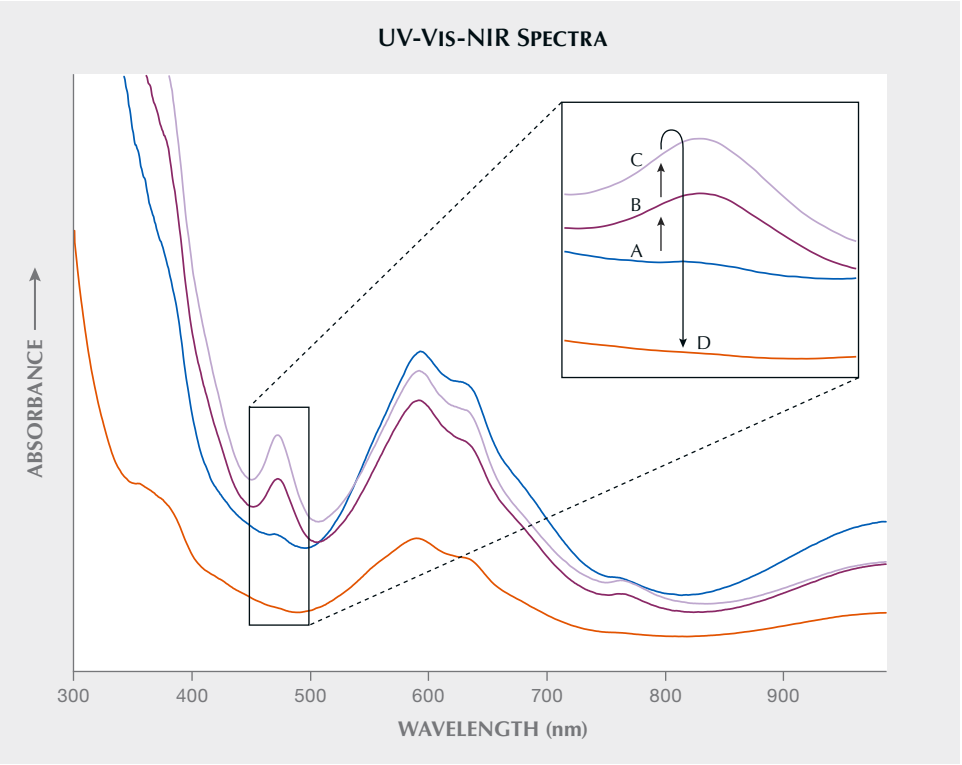

Figure 10. UV-Vis spectra of faceted sample 17407067 before and after heating experiments. The inset shows detail of the 475 nm band. The arrows in the inset show the order of experiments. Spectrum A was recorded from the as-received, nickel-diffused stone. Spectrum B was recorded after a 10-hour anneal at 1100°C in pure O_2. Spectrum C was recorded after an 18-hour anneal in pure O_2 at 1700°C. Spectrum D was recorded after a 40-hour anneal at 1750°C in a 2:1 H_2:CO_2 mix. Spectra were recorded in nearly the same position on the stone, so absorbance intensities are closely (but not exactly) comparable, as the stone's position was not perfectly reproduced in each case.

DISCUSSION

Nickel Incorporation Mechanism and Valence State. First, there are two likely valence states of nickel ions in spinel: Ni^{2+} and Ni^{3+}. The superscripts refer to the charges of the cation where Ni^{2+} has lost two electrons, and Ni^{3+} has lost three, relative to nickel in its

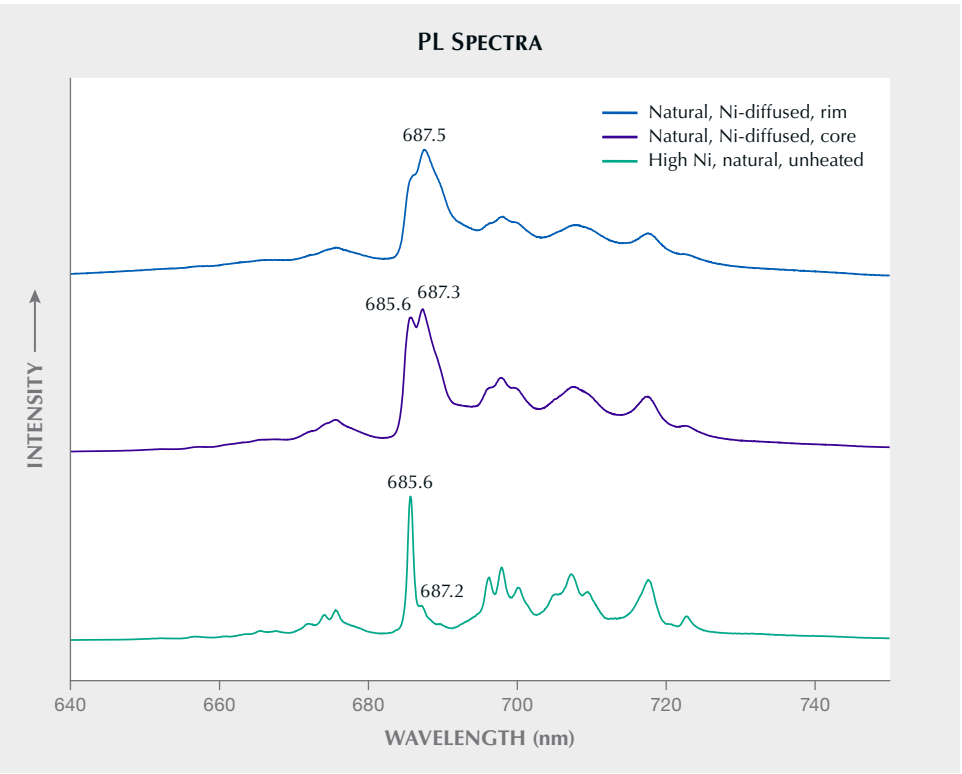

Figure 11. PL spectra recorded from the rim and core of a nickel-diffused natural spinel (sample 17407124), revealing features characteristic of heating. Also shown is a spectrum from a natural, unheated high-nickel spinel (>300 ppma nickel). Spectra are offset for clarity.

normal metallic state with zero charge. Because the loss of electrons is oxidation, the expected result is that, all other things being equal, a spinel treated with nickel in an oxidizing environment (generally an atmosphere having a high oxygen concentration, such as air), will have a relatively high ratio of Ni^{3+} to total nickel. Conversely, a spinel treated in a reducing (generally low-oxygen) atmosphere will have a relatively high ratio of Ni^{2+} to total nickel.

With two valence states, there are also two locations for nickel incorporation in spinel, either on the tetrahedral or octahedral site. The terms "tetrahedral" and "octahedral" refer to the location of these cations in the crystal structure with respect to the O^{2-} anions (ions with a negative charge). A cation in a tetrahedral site in spinel is bonded to four O^{2-} anions, forming the shape of a tetrahedron with the cation in the center. In octahedral coordination, the cation is bonded to six O^{2-} anions, which form an octahedron. These octahedra and tetrahedra stack together to form the atomic structure of spinel. Overall, then, there are four main possibilities for nickel incorporation, with two valence states (Ni^{2+} and Ni^{3+}) and two sites (octahedral and tetrahedral).

In natural spinel ($MgAl_2O_4$), which is likely to be the starting material for the diffusion treatment, Mg^{2+} mainly occupies the tetrahedral site, and Al^{3+} mostly occupies the octahedral site (O'Neill and Navrotsky, 1983; Widmer et al., 2015). This can be described as a low "degree of inversion." Chihmingite, $NiAl_2O_4$, is more complex because it tends toward an "inverse" spinel structure (having a high degree of inversion), meaning the octahedral sites are considerably occupied by Ni^{2+}, and Al^{3+} tends towards tetrahedral sites (Datta and Roy, 1967; Porta et al., 1974; O'Neill et al., 1991). This potentially means that a nickel-diffused spinel will show a degree of inversion that is intermediate between $MgAl_2O_4$ and $NiAl_2O_4$.

While we do not have sufficient information to fully assign valence states and sites to the nickel in these diffused spinel, we can make some speculations based on the data collected. First, from the LA-ICP-MS traverse and EDS maps, the decrease in nickel concentration from the rim to the core of the stones, coupled with magnesium showing the opposite trend, suggests nickel primarily replacing magnesium—i.e., Ni^{2+} and/or Ni^{3+} replacing Mg^{2+}.

Second, the main visible absorption bands in the spectra of the nickel-diffused spinel, at 597 and 639 nm, were assigned by, for example, Porta et al. (1974) and Serment et al. (2020), to nickel in tetrahedral coordination. The generally smaller bands at 369 and 381 nm were associated with nickel in octahedral coordination. The similarity between the absorption spectra of the nickel-diffused spinel and a spectrum of single-crystal nickel-doped spinel grown in a relatively low (but undefined) pO_2 argon atmosphere (figure 9; see also Jouini et al., 2007) suggests that the nickel is predominantly in its reduced form Ni^{2+}.

Third, the experimental results are useful for interpreting the 475 nm band, assigned by Sakurai et al. (1969) to nickel in tetrahedral coordination. This grew during a low-temperature (1100°C) anneal in pure O_2, suggesting that it relates to Ni^{3+}. During longer and higher-temperature anneals in pure O_2, the band did not increase further. When annealed at very low pO_2, the 475 nm band was completely eliminated, which would be consistent with Ni^{3+} being reduced to Ni^{2+}. Therefore, we can assign this band to Ni^{3+} with some confidence. As the 475 nm band absorbs in the visible range, this suggests that the color of a nickel-diffused spinel can be fine-tuned after treatment by a second oxidation or reduction treatment. Oxidation leads to more greenish hues, while reduction removes the green and shifts the color into a more exclusively blue hue.

Overall, the data suggest that the main nickel incorporation mechanism responsible for the spinel's color is Ni^{2+} replacing Mg^{2+} in tetrahedral coordination, shown by the 597 and 639 nm bands. The 475 nm band may be related to Ni^{3+} in tetrahedral coordination. However, this does not mean that all nickel is in tetrahedral coordination; in fact, it might only be a small fraction of the Ni^{2+} (e.g., Porta et al., 1974), although we cannot directly address this with our data.

This could explain the observation that nickel is apparently a weak chromophore in spinel. It is possible, however, that the main chromophore is Ni^{2+} in tetrahedral coordination, with a minor contribution of Ni^{3+}, but the majority of the nickel is Ni^{2+} in octahedral coordination.

Diffusivities. Fits of the compositional profiles for nickel, lithium, iron, zinc, vanadium, beryllium, cobalt, and magnesium to equation 1 (from the "Diffusion Modeling" section) are presented in figure 12, along with values of Dt (with units of m^2). These Dt values are also presented in figure 13. They increase in the following order: V<Ni<Mg<Fe≈Co<Zn≈Be<Li.

Because the durations (t) of the heat treatment of the stones studied are not known, it is not possible

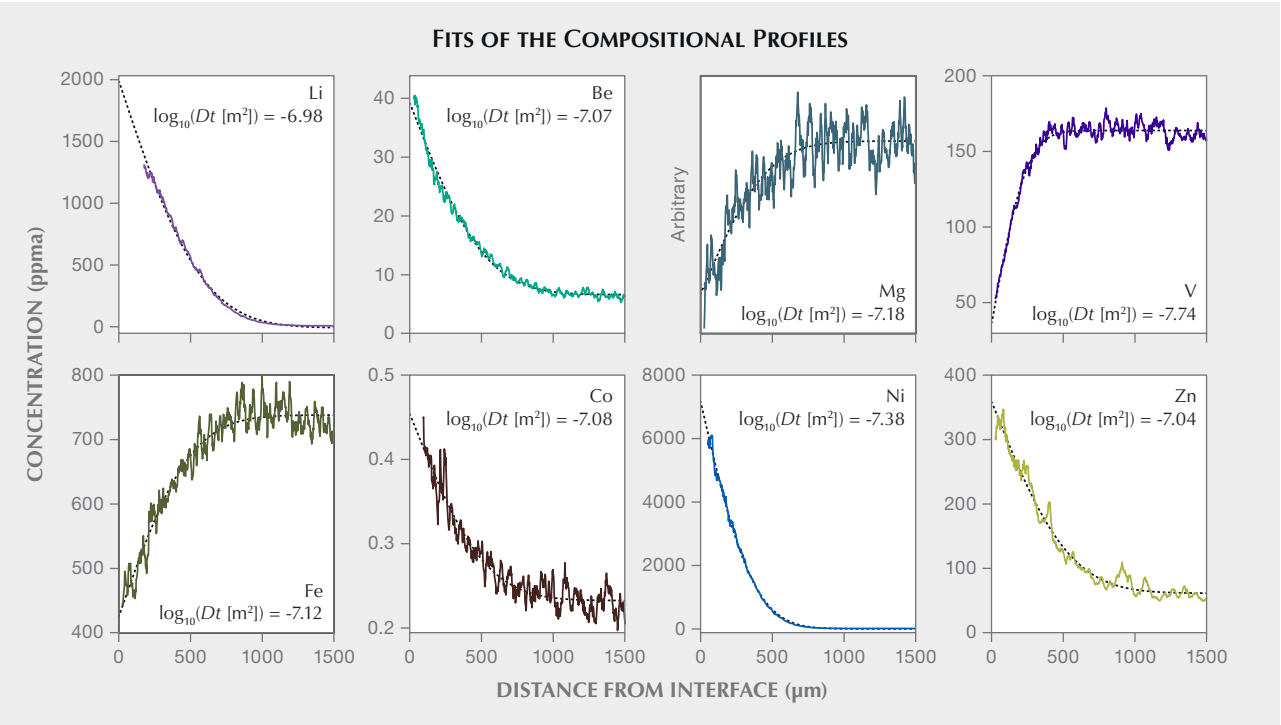

Figure 12. Profiles of lithium, beryllium, magnesium, vanadium, iron, cobalt, nickel, and zinc, as shown in figure 7, fitted to equation 1. Solid lines represent LA-ICP-MS data, while dashed lines represent the model fits. The "interface" is at the table of the stone. Also shown are the fitted values of Dt *(presented as their base-10 logarithm)—i.e., the diffusion coefficient multiplied by the time. Note that magnesium is not quantified, but this has no effect on the* Dt *value, which is independent of concentration according to equation 1.*

to precisely or accurately obtain D from Dt. Likewise, because the temperatures of the treatment are also not known to us, and because experimental datasets describing diffusion coefficients are extremely limited in any case, neither can t be determined using a known D. It is tempting to use the zonation in iron and magnesium to extract duration using iron and magnesium diffusion coefficients that have been determined experimentally (Sheng et al., 1992; Liermann and Ganguly, 2002), but the different measured D values for iron and magnesium lead to a 3–4 orders of magnitude discrepancy at temperatures over 1500°C, notwithstanding the usual potential inaccuracies associated with data extrapolation.

However, we can reasonably make two broad assumptions about the nature of the heat treatment. The first is that it is likely conducted at 1500–1700°C, the upper limit being both a safe temperature to avoid partial melting in a spinel with considerable concentrations of impurities (i.e., nickel) and the normal upper limit for continuous operation of standard high-temperature muffle furnaces with molybdenum disilicide elements. The lower limit is conservative—based on previously published data (e.g., Sheng et al., 1992), it is unlikely that diffusion can lead to hundreds of micrometers of diffusive penetration into the stone. Given the economics of treatment, we assume a short duration (again, extremely conservative) of one hour to one week.

With these very broad constraints, a range of D values for nickel can be estimated from Dt using t = 3600 s (1 hour) and 6×10^5 s (1 week). These can then be placed onto an Arrhenius diagram, which describes D (as its base-10 logarithm $\log_{10}D$, in m^2/s) as a function of temperature (as inverse temperature in Kelvins, $1/T$). This is shown in figure 13, along with some other experimentally determined diffusion coefficients for divalent cations in spinel as well as hydrogen for comparison. Also shown is the diffusion coefficient estimated for beryllium in corundum by

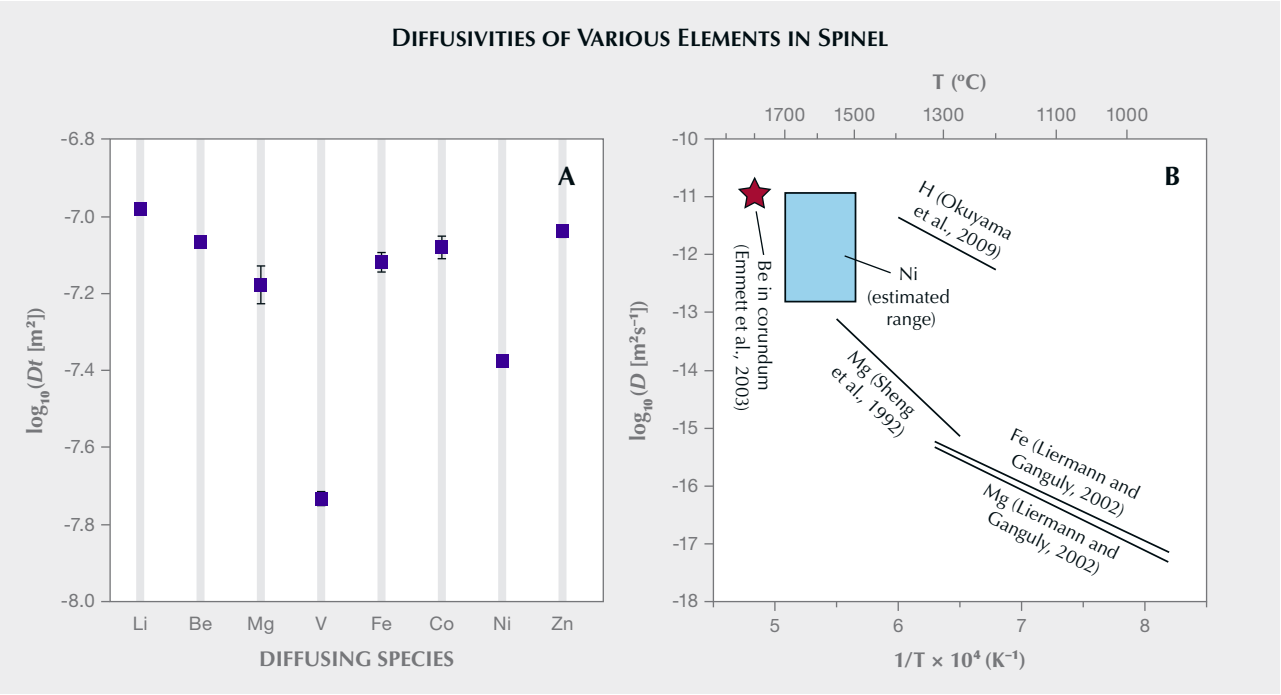

Figure 13. Results of fitting data to equation 1. Plot A shows the Dt *values from figure 12. Error bars represent 95% confidence intervals. Where not visible, the 95% confidence interval is smaller than the marker size. Vanadium has the lowest diffusivity and lithium the highest. Plot B shows some estimations of nickel diffusion coefficients extracted from the* Dt *values in plot A, making broad assumptions about treatment duration and temperature. These are presented on an Arrhenius diagram, with the base-10 logarithm of the diffusion coefficient plotted against the inverse temperature in K (temperatures in °C are presented at the top of the plot). Also shown are some experimentally determined diffusion coefficients for magnesium and iron (Sheng et al., 1992; Liermann and Ganguly, 2002), which can be expected to behave similarly to nickel in this system, and hydrogen (Okuyama et al., 2012), which is the fastest-diffusing element in many minerals. A diffusion coefficient of beryllium in corundum estimated by Emmett et al. (2003) is also included—this is important for a general understanding of diffusion treatment of gemstones.*

Emmett et al. (2003), which is pertinent for general considerations of heat treatment of gemstones. While these values are imprecise, they should provide a useful starting point for future experimental efforts.

The shapes of nickel diffusion profiles—i.e., the forms of concentration vs. distance data in figure 7—correspond almost perfectly to equation 1. This means that there is a smooth decrease in nickel concentration, and associated color, from the edge of a spinel to the core. This implies that diffusion in this system is relatively simple, with little or no trapping behavior—such non-simple behavior could be expressed as sharp color changes, as is often observed in titanium-diffused sapphires, for example. The likely diffusion mechanism would then involve a simple exchange of vacancies with Ni^{2+}, which has been proposed as one mechanism of Cr^{3+} diffusion in spinel (Posner et al., 2016).

Zonation Patterns. The zonation patterns extracted from the EDS map, shown in figure 8, can be used to provide some information regarding the heat treatment method. In the maps, we can see that the zonation patterns are broadly parallel to the edges of the stone, excluding the noise in the data. In other words, if contours were drawn defining regions of equal nickel concentration, they would generally have the same shape as the stone.

In a mineral with cubic symmetry (such as spinel), diffusion treatment will lead to concentration contours that are smooth but generally parallel to the edges of the stone, regardless of the stone's geometry. An example is shown in figure 14, where diffusion has been modeled in a simplified two-dimensional system for both a faceted shape and an example "rough" shape. If faceting is done before the diffusion treatment, then the contours of equal concentration will essentially match the shape of the faceted stone. This is what is

seen in the nickel-diffused spinel, as in figure 8. However, if the diffusion treatment is done on a rough stone that is subsequently faceted, the contours will likely be intersected by the newly cut surface. In the example in figure 14, this would lead to a patchy appearance, with the degree of patchiness dependent on the relative geometries of the rough and faceted stones.

What cannot be accurately determined using our data, though, is whether the faceting done before the diffusion treatment was complete or partial. The diffusion treatment could have been done on a partially faceted, unpolished stone, with final faceting and polishing after the treatment.

To demonstrate this process, two flame-fusion synthetic spinels were diffused with nickel at 1800°C in a furnace at GIA in Carlsbad, California. The two stones were completely colorless beforehand and facet patterns were roughly ground in. Diffusing these stones with nickel at 1800°C created a rich blue color as seen in the polished gems in figure 15.

It is also notable that local color concentrations were visible at facet junctions, which is consistent with diffusion treatment conducted after faceting.

Speculations Regarding the Heat Treatment Method. The most salient lines of evidence in determining the heat treatment method are:

- The presence of high nickel and lithium concentrations at the stone's edge.
- The lower trace and minor element contents in the core (e.g., beryllium and zinc), relative to the edge, measured using an LA-ICP-MS transect.
- The PL spectra, which are consistent with heated natural spinel.
- The presence of healed fractures.
- The presence of a band in the UV-Vis-NIR spectra of all measured stones at 475 nm, which can be removed by annealing at low pO_2.

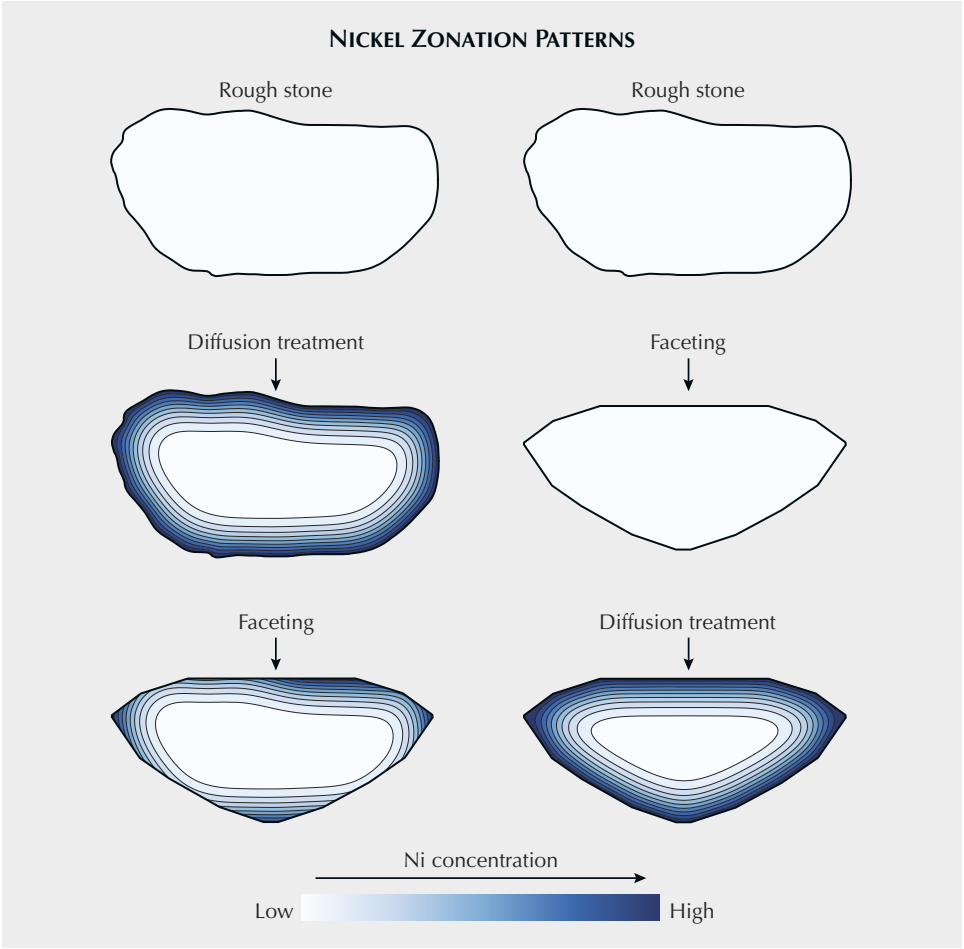

Figure 14. Models showing the nickel zonation patterns that would be observed with diffusion treatment done before (left column) or after (right column) faceting, using a generic "rough" shape. The zonation pattern broadly follows the shape of the stone, which would then be retained if the stone were faceted after diffusion treatment. These models were created using an explicit finite difference approximation of Fick's second law in two dimensions, using an arbitrary initial concentration of 0 and a constant boundary concentration of 1. Contours are at intervals of 0.1, from 0.0 to 1.0. The girdle-to-girdle length in the model is 4 mm, the grid spacing is 10 µm, the modeled D *is* 10^{-13} m^2/s*, and the total modeled time is* 2×10^6 *s.*

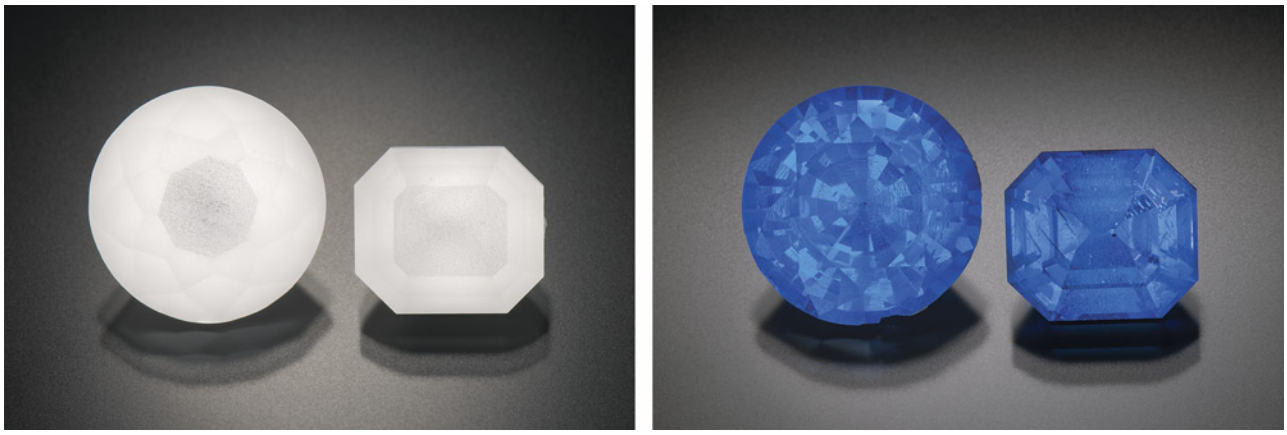

Figure 15. Two synthetic spinels before and after a diffusion experiment carried out at GIA in Carlsbad, California. The stones were faceted by Jessa Rizzo (GIA) and weigh 9.25 and 14.72 ct. Photos by Kevin Schumacher.

- The long diffusive penetration distances (over 1 mm).
- The nickel concentration variations in the EDS map, where zonation is approximately parallel to the edges of the stone.
- The fact that the stones were mixed into a parcel of cobalt-diffused spinel and sold as such.

Overall, the evidence suggests the treatment of natural faceted or partially faceted spinel in the presence of a high-nickel melt, where some lithium compound is used to enable flux melting. This is often advantageous because any adhered melt can be readily dissolved off the stone after treatment. As described above, the treatment is likely at high temperature (>1500°C), given the depth of the diffusion profiles as well as considerations of the economics of heat treatment. The presence of the 475 nm band suggests that the treatment was done in an oxidizing atmosphere, which could simply be air, because this band is eliminated if annealed in a reducing gas mix.

Finally, there is a possibility that the use of nickel rather than cobalt as a diffusant was accidental, or alternatively that the term "cobalt-diffused" is now used by some treaters as a generic term for diffusion treatment in spinel.

CONCLUSIONS

Blue or green hues can be added to spinel by nickel diffusion. Spinel modified using this treatment method now exists in the gem trade. The possibility for color modification by nickel diffusion should be considered for any spinel with such colors. The following criteria are proposed for identifying nickel diffusion treatment in spinel:

- High concentrations of nickel at the stone's surface, potentially thousands of atomic parts per million or more. This may be associated with high lithium concentrations.
- PL spectra characteristic of heated natural spinel, although we cannot rule out the possibility of treatment of lab-grown spinel.
- Characteristic UV-Vis absorption spectra, with bands at around 370, 470, and 600 nm.
- Subtle color concentrations at the facet junctions, although this may be limited if the stones are repolished after treatment.
- Textures associated with flux-assisted healing of fractures.

Overall, the treatment should be readily identifiable using standard gemological techniques and equipment.

ABOUT THE AUTHORS

Dr. Michael Jollands, Abadie Ludlam, Pamela Cevallos, Sarah Arden, Elina Myagkaya, and Dr. Ulrika D'Haenens-Johannson are researchers with GIA in New York. Dr. Aaron Palke, Dr. Shiyun Jin, and Ziyin Sun are with GIA in Carlsbad. Wim Vertriest and Vararut Weeramongkhonlert are with GIA in Bangkok.

REFERENCES

Crank J. (1975) *The Mathematics of Diffusion*. Oxford University Press, Oxford, UK.

Datta R.K., Roy R. (1967) Equilibrium order-disorder in spinels. *Journal of the American Ceramic Society*, Vol. 50, No. 11, pp. 578–583, http://dx.doi.org/10.1111/j.1151-2916.1967.tb15002.x

Emmett J.L., Scarratt K., McClure S.F., Moses T., Douthit T.R., Hughes R., Novak S., Shigley J.E., Wang W., Bordelon O., Kane R.E. (2003) Beryllium diffusion of ruby and sapphire. *G&G*, Vol. 39, No. 2, pp. 84–135, http://dx.doi.org/10.5741/GEMS.39.2.84

Jochum K.P., Weis U., Stoll B., Kuzmin D., Yang Q., Raczek I., Jacob D.E., Stracke A., Birbaum K., Frick D.A., Günther D., Enzweiler J. (2011) Determination of reference values for NIST SRM 610–617 glasses following ISO guidelines. *Geostandards and Geoanalytical Research*, Vol. 35, No. 4, pp. 397–429, http://dx.doi.org/10.1111/j.1751-908X.2011.00120.x

Jouini A., Yoshikawa A., Guyot Y., Brenier A., Fukuda T., Boulon G. (2007) Potential candidate for new tunable solid-state laser between 1 and 2µm: Ni^{2+}-doped $MgAl_2O_4$ spinel grown by the micro-pulling-down method. *Optical Materials*, Vol. 30, No. 1, pp. 47–49, http://dx.doi.org/10.1016/j.optmat.2006.11.027

Krzemnicki M., Wang H., Stephan T., Henn U. (2017) Cobalt diffusion treated spinel. *Proceedings of the 35th International Gemmological Conference*, Windhoek, Namibia.

Liermann H.-P., Ganguly J. (2002) Diffusion kinetics of Fe^{2+} and Mg in aluminous spinel: Experimental determination and applications. *Geochimica et Cosmochimica Acta*, Vol. 66, No. 16, pp. 2903–2913, http://dx.doi.org/10.1016/S0016-7037(02)00875-X

Longerich H., Jackson S., Gunther D. (1996) Inter-laboratory note: Laser ablation inductively coupled plasma mass spectrometric transient signal data acquisition and analyte concentration calculation. *Journal of Analytical Atomic Spectrometry*, Vol. 11, No. 9, pp. 899–904, http://dx.doi.org/10.1039/JA9961100899

Lorenzi G., Baldi G., Di Benedetto F., Faso V., Lattanzi P., Romanelli M. (2006) Spectroscopic study of a Ni-bearing gahnite pigment. *Journal of the European Ceramic Society*, Vol. 26, No. 3, pp. 317–321, http://dx.doi.org/10.1016/j.jeurceramsoc.2004.10.027

Miyawaki R., Hatert F., Pasero M., Mills S.J. (2022) IMA Commission on New Minerals, Nomenclature and Classification (CNMNC) – Newsletter 69. *European Journal of Mineralogy*, Vol. 34, No. 5, pp. 463–468, http://dx.doi.org/10.5194/ejm-34-463-2022

O'Neill H.S.C., Dollase W.A., Ross C.R. (1991) Temperature dependence of the cation distribution in nickel aluminate ($NiAl_2O_4$) spinel: A powder XRD study. *Physics and Chemistry of Minerals*, Vol. 18, No. 5, pp. 302–319, http://dx.doi.org/10.1007/BF00200188

O'Neill H.S.C., Navrotsky A. (1983) Simple spinels: crystallographic parameters, cation radii, lattice energies, and cation distribution. *American Mineralogist*, Vol. 68, No. 1-2, pp. 181–194.

Okuyama Y., Kurita N., Sato D., Douhara H., Fukatsu N. (2012) Determination of the maximum solubility of hydrogen in α-alumina by DC polarization method. *Solid State Ionics*, Vol. 213, pp. 92–97, http://dx.doi.org/10.1016/j.ssi.2011.05.023

Paton C., Hellstrom J., Paul B., Woodhead J., Hergt J. (2011) Iolite: Freeware for the visualisation and processing of mass spectrometric data. *Journal of Analytical Atomic Spectrometry*, Vol. 26, No. 12, pp. 2508–2518, http://dx.doi.org/10.1039/c1ja10172b

Peretti A., Kanpraphai-Peretti A., Günther D. (2015) New type of treatment of spinel involving heat-treatment and cobalt diffusion. In World of Magnificent Spinels: Provenance and Identification. *Contributions to Gemology*, No. 11, pp. 279–282.

Porta P., Stone F.S., Turner R.G. (1974) The distribution of nickel ions among octahedral and tetrahedral sites in $NiAl_2O_4$-$MgAl_2O_4$ solid solutions. *Journal of Solid State Chemistry*, Vol. 11, No. 2, pp. 135–147, http://dx.doi.org/10.1016/0022-4596(74)90108-X

Posner E.S., Ganguly J., Hervig R. (2016) Diffusion kinetics of Cr in spinel: Experimental studies and implications for ^{53}Mn–^{53}Cr cosmochronology. *Geochimica et Cosmochimica Acta*, Vol. 175, pp. 20–35, http://dx.doi.org/10.1016/j.gca.2015.11.018

Prunier A.R., Hewitt D.A. (1981) Calculation of temperature-oxygen fugacity tables for H_2-CO_2 gas mixtures at one atmosphere total pressure. *Geological Society of America Bulletin*, Vol. 92, No. 7 Part II, pp. 1039–1068, http://dx.doi.org/10.1130/GSAB-P2-92-1039

Saeseaw S., Weeramonkhonlert V., Khowpong C., Ng-Pooresatien N., Sangsawong S., Raynaud V., Ito C. (2015) Cobalt diffusion of natural spinel: A report describing a new treatment on the gem market. *GIA News from Research*, June 3, https://www.gia.edu/doc/Cobalt-Diffusion-in-Spinel-v2.pdf

Sakurai T., Ishigame M., Arashi H. (1969) Absorption spectrum of Ni^{2+} ions in spinel. *Journal of Chemical Physics*, Vol. 50, No. 8, pp. 3241–3245, http://dx.doi.org/10.1063/1.1671546.

Serment B., Gaudon M., Demourgues A., Noël A., Fleury G., Cloutet E., Hadziioannou G., Brochon C. (2020) Cyan $Ni_{1-x}Al_{2+2x/3}\square_{x/3}O_4$ single-phase pigment synthesis and modification for electrophoretic ink formulation. *ACS Omega*, Vol. 5, No. 30, pp. 18651–18661, http://dx.doi.org/10.1021/acsomega.0c01289

Shannon R. (1976) Revised effective ionic radii and systematic studies of interatomic distances in halides and chalcogenides. *Acta Crystallographica Section A: Crystal Physics, Diffraction, Theoretical and General Crystallography*, Vol. 32, No. 5, pp. 751–767, http://dx.doi.org/10.1107/S0567739476001551

Sheng Y.J., Wasserburg G.J., Hutcheon I.D. (1992) Self-diffusion of magnesium in spinel and in equilibrium melts: Constraints on flash heating of silicates. *Geochimica et Cosmochimica Acta*, Vol. 56, No. 6, pp. 2535–2546, http://dx.doi.org/10.1016/0016-7037(92)90207-Y

Widmer R., Malsy A.-K., Armbruster T. (2015) Effects of heat treatment on red gemstone spinel: single-crystal X-ray, Raman, and photoluminescence study. *Physics and Chemistry of Minerals*, Vol. 42, No. 4, pp. 251–260, http://dx.doi.org/10.1007/s00269-014-0716-7